FeMn/Fe/Co/Cu(1,1,10) films studied using the magneto-optic Kerr effect and photoemission electron microscopy

Y. Meng, J. Li, A. Tan, J. Park, E. Jin, H. Son, A. Doran, A. Scholl, E. Arenholz, H. W. Zhao, Chanyong Hwang, and Z. Q. Qiu

Phys. Rev. B **84**, 064416 — Published 19 August 2011

DOI: 10.1103/PhysRevB.84.064416

A study of FeMn/Fe/Co/Cu(1,1,10) films using MOKE and XMCD

Y. Meng,[1,2] J. Li,[1] A. Tan,[1] J. Park, [1] E. Jin,[1] H. Son,[1] A. Doran,[3] A. Scholl,[3] E. Arenholz,[3] H. W. Zhao,[2] Chanyong Hwang,[4] and Z. Q. Qiu[1]

[1] *Department of Physics, University of California at Berkeley, Berkeley, California 94720, USA*

[2] *Institute of Physics, Chinese Academy of Science, Beijing, 100190, P. R. China*

[3] *Advanced Light Source, Lawrence Berkeley National Laboratory, Berkeley, California 94720, USA*

[4] *Korea Research Institute of Standards and Science, Yuseong, Daejeon 305-340, Korea*

Abstract

FeMn/Fe/Co/Cu(1,1,10) films were grown epitaxially and investigated using Magneto-Optic Kerr Effect and Photoemission Electron Microscopy. We found that the FeMn/Fe/Co/Cu(1,1,10) exhibits the same property as FeMn/Co/Cu(1,1,10) for ferromagnetic phase of the fcc Fe film, but a different property for non-ferromagnetic phase of the fcc Fe film. The result indicates that the characteristic property reported in the literature for FeMn/Co/Cu(001) comes from the FeMn spin structure, and is independent of the ferromagnetic layer.

PACS numbers: 75.70.Ak

I. Introduction

Antiferromagnetic (AFM)/ferromagnetic (FM) bilayer system has been studied extensively because of the application of the exchange bias effect in magnetic read head devices [1,2]. Despite the importance of the AFM/FM system in technology, the AFM/FM interfacial interaction is much more complicated than the FM/FM interfacial interaction because of the magnetic frustration that the nearest neighbor interaction energy cannot be minimized for all pairs of spins at the same time [3]. The magnetic interfacial frustration becomes even more complicated when interfacial roughness is present in real experimental systems. In theory, various models have been applied to deal with the interfacial frustration such as the spin-flop AFM/FM coupling [4] and the random field model [5]. In experiment, AFM/FM system has been studied with the AFM layer being either oxide or metallic thin films. The advantage/disadvantage of these two classes is that oxide AFM films can be measured by the X-ray Magnetic Linear Dichroism (XMLD) but usually suffer a rougher and interdiffusive interface, and that metallic AFM films have a sharper interface but a vanishing of the XMLD signal. While the latter has been widely applied to magnetic devices, investigation on its interfacial AFM/FM interaction has been progressed rather slowly. FeMn film is one representative metallic AFM system because of its excellent epitaxial growth on Cu(001) substrate and its interesting AFM/FM interfacial interaction. For example, FeNi/FeMn bilayer system exhibits characteristic FeNi spin spiral structure and chirality during the FeNi magnetic reversal [6,7]. Various types of magnetic anisotropies (e.g. unidirectional, uniaxial, and 4-fold anisotropies) can also be generated by the FeMn/FM spin frustration in different thickness ranges [8,9]. The FeMn layer could even have a lateral effect on a FM layer underneath it [10]. In an effort to classify the FeMn/FM interfacial interaction, single crystalline FeMn/Co/Cu(001) thin films have become important because of the excellent epitaxial growth [11,12]. It was shown that the FeMn films exhibit three dimensional noncollinear antiferromagnetic spin structure [13] that significantly affects the Co magnetization at the FeMn paramagnetic-to-antiferromagnetic transition [14,15]. The observed phenomena have two distinct characteristics: (1) the Co magnetic domains break into small sized domains at the FeMn paramagnetic-to-antiferromagnetic transition, and (2) the Co easy magnetization axis switches in the film plane by 45^{o} from the

Co[110] axis at FeMn paramagnetic state to the Co[100] axis at FeMn antiferromagnetic state. The above result has been attributed to the FeMn noncollinear spin structure that uncompensated FeMn spins at the [100] atomic steps are coupled to the local Co spins. Subsequent studies on FeMn/Co films grown on vicinal Cu(001) substrate with [110] and [100] steps support that [100] steps indeed have a stronger effect on the Co magnetization than [110] steps [16]. It was also shown that a FeMn layer could interact with another FeMn/FM bilayer across a Cu spacer layer [17]. Although the later works on epitaxial FeMn/FM thin films have fruitful results such as the effect of induced Fe moment [18] and the magnetic anisotropies [19,20], it has not been addressed that if the observed properties, especially the in-plane 45^o spin switching of the Co mentioned above, are unique to the FeMn/Co interfacial interaction? Specifically, does the Co 45^o spin switching depend on the FeMn spin structure only or also depend on the FM layer property? To address this issue, it would be best to insert a spacer layer between the FeMn and the Co layers and to switch the spacer layer between different magnetic states to intermediate different types of FeMn-Co interactions. For this purpose, we carried out an investigation on FeMn/Fe/Co/vicinal Cu(001) using magneto-optical Kerr effect (MOKE) and photoemission electron microscope (PEEM). By changing the magnetic state of the fcc Fe spacer layer from FM phase into non-ferromagnetic phase, we show that the Co spin direction undergoes a 45^o spin switching only for FM phase of the fcc Fe film, and remains unswitched for non-ferromagnetic phase of the fcc Fe. This result supports the argument that the 45^o spin switching of the Co film is associated to the FeMn local spin structure [14].

2. Experiment

A Cu (1, 1, 10) single crystal substrate, which has atomic steps parallel to the [110] axis, was mechanically polished followed by electrochemical polishing under a constant voltage of 1.8V for 15 seconds in a mixture of liquid solution of 75% phosphoric acid, 10% sulfuric acid, and 15% water. [21] The Cu substrate was then transferred into an ultrahigh vacuum chamber with a base pressure of $2x10^{-10}$ torr, and cleaned by cycles of Ar ion sputtering at ~ 2kV and annealing at ~600^{o}C. A 20 monolayer (ML) Co film was deposited on top of the Cu substrate and followed by a double cross wedges of Fe

(0~12ML) and FeMn (0~20ML) to form the sample of FeMn(wedge)/Fe(wedge)/Co(20ML)/Cu(1,1,10). The wedges were grown by moving the substrate behind a knife-edge shutter during the film growth to permit a continuous change of the Fe and FeMn Fe thicknesses. The two wedges are orthogonal to each other so that their thicknesses can be changed independently. The FeMn film was grown by co-evaporating Fe and Mn with equal evaporation rates to form a 50-50 composition alloy of $Fe_{50}Mn_{50}$. The Cu substrate and the sample were characterized by Low Energy Electron Diffraction (LEED). Figure 1 shows the LEED patterns of the FeMn/Fe/Co/Cu(1,1,10) at different stages of the growth. Since the FeMn and Fe are wedges, we can only roughly estimate that the LEED patterns are from ~2ML Fe and ~10ML FeMn. Clear split LEED spots are present, showing the formation of regular atomic steps on the vicinal surface. The LEED spot splitting is as sharp as the Cu substrate for the Co film but becomes a little bid blurred for the Fe and FeMn films, indicating a fluctuation of the vicinal steps or the film roughness of the Fe and FeMn films. Nevertheless, the existence of the LEED patterns for all the layers shows the epitaxial growth of the fcc Co, Fe, and FeMn layers in this system.

A 30Å Cu layer was grown on top of the sample to protect it from contamination. Magnetic hysteresis loops of the film were measured *in situ* by Magneto-Optic Kerr Effect (MOKE) using a He-Ne laser at an incident angle of 45^o to the sample surface [21]. After MOKE measurement, the sample was transferred into the PEEM chamber at beam line 7.3.1.1 of the Advanced Light Source (ALS) at the Lawrence Berkeley National Laboratory. The sample was demagnetized in an AC magnetic field (50 Hz) by gradually reducing the field strength to zero. The x-ray beam was circularly polarized and incident at an angle of 60^o relative to the sample surface normal direction. The magnetic domain images were obtained using Photoemission Electron Microscopy (PEEM) by taking the ratio of the Co and Fe L_3 and L_2 absorption edges, utilizing the effect of X-ray Magnetic Circular Dichroism (XMCD) [16].

3. Results and Discussion

MOKE measurements were taken at different Fe and FeMn thicknesses. No MOKE loops were detectable for magnetic field applied perpendicular to the film plane,

showing that the magnetization of the sample is in the film plane in all studied thickness ranges. Thus all the hysteresis loops in this paper are for magnetic field in the film plane. It is well known that fcc Fe film on Cu(001) and Co(001) is ferromagnetic (FM) for $0<d_{Fe}<4$ML and antiferromagnetic (AFM) for $5ML<d_{Fe}<11$ML [22,23]. We took MOKE measurement in the range of $0<d_{Fe}<4$ML and $5ML<d_{Fe}<11$ML and didn't find obvious difference within each range. Therefore, we show MOKE and PEEM results at d_{Fe}=2ML and d_{Fe}=8ML to represent the FM and AFM phases of the fcc Fe film.

Figure 2 (a) displays magnetic hysteresis loops of FeMn/Fe(2ML)/Co(20ML)/Cu(1,1,10) at room temperature. At thin FeMn region, the hysteresis loop exhibits a square shape with a full remanence for magnetic field applied parallel to the atomic steps but two split loops with a zero remanence for magnetic field applied perpendicular to the steps. This observation shows that the FeMn/Fe(2ML)/Co(20ML)/Cu(1,1,10) carries a uniaxial magnetic anisotropy that favors the Fe/Co magnetization parallel to the atomic steps of the vicinal surface, consistent with the Co/vicinal Cu(001) result [21]. As the FeMn film thickness (d_{FeMn}) increases, the coercivity of the film for magnetic field parallel to the steps (easy magnetization axis) increases significantly [Figure. 2 (a)] at $d_{FeMn}>11$ML. For magnetic field perpendicular to the steps (hard magnetization axis), the hysteresis loops remains split-loop character until $d_{FeMn}>11$ML above which the coercivity increases dramatically to overwhelm the split-loop character, making the loop similar to that for magnetic field parallel to the steps [Figure 2 (a)]. The coercivity for magnetic field along the easy magnetization axis is shown in Fig. 2(c) to better view the dramatic increase at $d_{FeMn}>11$ML. The result shown in Fig. 2(a) and (c) is the same as that of FeMn/Co/vicinal Cu(001) [16], suggesting that the hysteresis loop evolution with the FeMn thickness has the same origin as in the FeMn/Co/vicinal Cu(001) system. In the latter case, the physical origin has been attributed to the establishment of the AFM order in FeMn film at $d_{FeMn}>11$ML [14,16].

We then performed MOKE measurement on FeMn/Fe(8ML)/Co/vicinal Cu(001) in which the 8ML Fe represents the AFM phase of the fcc Fe film. To ensure that we obtain information on the AFM state of the fcc Fe, we measured the film at both room temperature and at T=90K. Fig. 2(b) shows the hysteresis loops of the sample at T=90K at different FeMn thicknesses. The split and square loops for magnetic field applied

perpendicular and parallel to the steps show the existence of a uniaxial magnetic anisotropy. The coercivity of the easy axis loop increases slightly with increasing the FeMn thickness above d_{FeMn}~7-10ML, showing the effect of the FeMn AFM order on the Co coercivity. However, there are two major differences as compared to the 2ML Fe sample. First, the easy axis for FeMn/Fe(8ML)/Co(20ML)/vicinal Cu(001) is perpendicular to the vicinal steps, opposite to the FeMn/Fe(2ML)/Co(20ML)/vicinal Cu(001) case which has its easy magnetization axis parallel to the steps. It is well known that step-induced anisotropy depends on the chemical bonding at the step edges. However, it is not predictable yet on the easy magnetization axis direction, neither to the effect of foreign atom absorption at the step edges [24]. Thus the different easy axis directions for the 2ML Fe sample and 8ML Fe sample show that the AFM or non-ferromagnetic and FM phases of the fcc Fe film have a very different effect on the step-induced magnetic anisotropy in Fe/Co/vicinal Cu(001). Detailed mechanism is unknown and relies on future study. Second, although the coercivity of the FeMn/Fe(8ML)/Co(20ML)/vicinal Cu(001) sample increases with increasing the FeMn thickness above its AFM ordering thickness [Fig. 2(b) and (c)], the easy magnetization axis remains in the perpendicular direction of the steps instead of processing a 45^o switching as in the d_{Fe}=2ML sample. The coercivity increase in FeMn/Fe(8ML)/Co(20ML)/vicinal Cu(001) at thicker FeMn is also smaller than in FeMn/Fe(2ML)/Co(20ML)/vicinal Cu(001) sample, indicating a weakened FeMn-Co coupling across the 8ML Fe film as compared to 2ML Fe film. Room temperature result is similar to T=90K result except the splitting field for the hard axis loop and the coercivity for the easy axis loop is slightly smaller at room temperature than at T=90K (the coercivity at room temperature is also plotted in Fig. 2(c) for comparison). This could be explained by the fact that the Néel temperature of fcc Fe film in the 4-10ML range is very close to room temperature [22]. The result in the 8ML Fe sample shows that the AFM or non-ferromagnetic phase of fcc Fe mediates the FeMn/Co interaction differently from the FM fcc Fe.

FeMn has a 3Q-like spin structure [25] which results in an uncompensated magnetic spins at [100] type steps on (001) surface. Then a direct coupling of the Co spins to the FeMn uncompensated spins at the [100] steps explains why the Co spin

switches from the [110] axis at the paramagnetic state of the FeMn film to the [100] axis at the AFM state of the FeMn film in FeMn/Co/Cu(001) [14-16]. The above physical mechanism comes from the spin structure of the FeMn and should be independent of the FM spin structure. Therefore for FM fcc Fe, the FeMn/Fe interfacial interaction should be the same as the FeMn/Co interfacial interaction. Then the direct FM collinear coupling between FM Fe and Co layers would naturally lead to the same FeMn/Co and FeMn/[Fe(2ML)/Co] interfacial interactions. For non-ferromagnetic fcc Fe, however, the FeMn-Co coupling has to take place across the fcc Fe spacer layer so that the FeMn-Co coupling should be significantly weakened to result in a different Co behavior than the FeMn/Co bilayer especially if the fcc Fe does not inherit the FeMn 3Q spin structure. In fact, it is know that the AFM phase of the fcc Fe film has a spin-density wave structure [26] which is very different from the FeMn 3Q spin structure. That explains why we observed the same behavior for FeMn/Fe(2ML)/Co(20ML)/vicinal Cu(001) but a different behavior for FeMn/Fe(8ML)/Co(20ML)/vicinal Cu(001) as compared to the FeMn/Co(20ML)/vicinal Cu(001). In fact, effect of a nonmagnetic Cu spacer layer between FeMn and Co has been studied by Wang et. al [27], and it was found that the Cu layer indeed weakens significantly the FeMn-Co coupling to affect the Co domain size and the domain diminishing field strength. The much weaker coercivity enhancement in FeMn/Fe(8ML)/Co than FeMn/Fe(2ML)/Co samples is consist with a weaker FeMn-Co coupling across 8ML Fe than 2ML Fe films. To further test this mechanism microscopically for fcc Fe spacer layer, we took magnetic domain images of FeMn/Fe/Co(20ML)/vicinal Cu(001) using PEEM at d_{Fe}=2ML and d_{Fe}=8ML. The sample was first demagnetized within an AC magnetic field to create domains. We first confirmed that FM fcc Fe and induced FM Fe in AFM phase of fcc Fe [28] are coupled ferromagnetically to the Co as they always have the same domains (Fig. 3). Thus we took Co domain images to represent the Fe/Co layer domains in this paper.

PEEM images were then taken with the in-plane projection of the incident x-rays parallel and perpendicular to the vicinal steps. We first discuss the PEEM result for FeMn/Fe(2ML)/Co/vicinal Cu(001) where the fcc Fe is at the FM state. At d_{FeMn}=5ML, we observe domains with two colors when the in-plane projection of the incident x-ray is parallel to the vicinal steps [top row of Fig. 4(a)]. The domain contrast vanishes as the

in-plane projection of the incident x-ray becomes perpendicular to the steps [lower row of Fig. 4(a)]. Recalling that the XMCD measures the projection of the magnetization along the x-ray direction, the above result shows that the Fe/Co magnetization is parallel to the vicinal steps, consistent with the MOKE measurement result. The small portion of domains with magnetization perpendicular to the steps represents metastable state domains left by the demagnetization process. As the FeMn thickness increases to 8ML, the majority domains remain in the state with the magnetization parallel to the steps but a small portion of the sample switches the magnetization to the direction perpendicular to the steps [grey region in the top image and dark region in the lower image of Fig. 4(a) at d_{FeMn}=8ML]. At d_{FeMn}=11ML, the domain breaks into small sized domains which resembles the characteristics of the FeMn/Co/Cu(001) at the AFM ordering point of the FeMn film [14-17]. For d_{FeMn}>11ML, the domains are visible for x-rays in both directions. By comparing the shape and contrast, it is easy to identify that the magnetizations in these domains are 45^o from the vicinal step direction, i.e., along the [±1,0,0] and [0,±1,0] directions [16]. The above domain evolution is identical to our previous observation in FeMn/Co/vicinal Cu(001) system [16]. Therefore we conclude that FeMn/Fe(2ML)/Co/vicinal Cu(001) has the same property as the FeMn/Co/vicinal Cu(001), i.e., the FM phase of the fcc Fe results in an identical FeMn/[Fe/Co] interfacial interaction as FeMn/Co. In another word, the FeMn/FM interfacial interaction is determined by the AFM spin structure of the FeMn and is independent of the FM layer.

We now present the PEEM result of FeMn/Fe(8ML)/Co(20ML)/vicinal Cu(001) to reveal the effect of the non-ferromagnetic phase of the fcc Fe film on the FeMn/Co interaction. It should be mentioned that fcc Fe in the 4-8ML range has a Néel temperature at or just below the room temperature [22,26]. Since we can only perform PEEM measurement at room temperature, our PEEM result should represent the fcc Fe close or at the AFM phase. On the other hand, our MOKE result doesn't show significant difference between 300K and 90K, we believe the PEEM result more likely represents the property of AFM fcc Fe. Nevertheless, the essential point here is to compare the different effects of FM fcc Fe (2ML) and non-ferromagnetic fcc Fe (8ML), we here use "non-ferromagnetic" phase to represent the 8ML Fe at room temperature. Fig. 4(b) shows the PEEM result of FeMn/Fe(8ML)/Co(20ML)/vicinal Cu(001). Domains with two

colors are observed as the in-plane projection of the x-ray is perpendicular to the vicinal steps, and the domain contrast disappears as the incident x-ray is parallel to the steps. This result agrees with the MOKE result that the easy magnetization axis is now perpendicular to the vicinal steps. The most important observation is that the domains don't change their character as d_{FeMn} increases, i.e., the change of the domain size at d_{MnFe}=11ML and the 45^o Co spin switching at d_{MnFe}>11ML in the d_{Fe}=2ML sample no longer exist in the d_{Fe}=8ML sample. This result confirms the MOKE result that the non-ferromagnetic phase of the fcc Fe film produces a very different result than the FM phase Fe in the FeMn/Fe/Co/vicinal Cu(001) system. As mentioned earlier, the AFM phase of the fcc Fe has a spin-density wave structure [26] which is very different from the FeMn 3Q spin structure. Then the disappearance of the FeMn/Co interfacial interaction character after inserting an 8ML fcc Fe layer shows that the FeMn 3Q spin structure at the FeMn/Fe(8ML) interface dissolves in the non-ferromagnetic phase fcc Fe and no longer affects the Co layer in the way as it is in the FeMn/Fe(2ML) case. In another word, the small domain size of Co at the AFM order point of the FeMn (d_{FeMn}=11ML) and the 45^o spin switching of the Co at d_{FeMn}>11ML indeed come from the FeMn spin structure.

IV Summary

In summary, we investigated the magnetic properties of FeMn/Fe/Co/vicinal Cu(001) using MOKE and PEEM. For FM phase of Fe, the FeMn/Fe/Co/Cu(1,1,10) exhibits the same property as FeMn/Co/vicinal Cu(001), i.e., the Co film changes into small sized domains at the AFM ordering point of the FeMn film and switches the spin direction by 45^o above the FeMn AFM ordering thickness. For non-ferromagnetic phase of the fcc Fe, the Co easy magnetization axis changes to perpendicular to the vicinal steps and remains in that direction as the FeMn thickness increases to establish its AFM order. This result proves that the characteristic FeMn/Co interfacial interaction indeed comes from the FeMn spin structures.

Acknowledgement

This work is supported by National Science Foundation DMR-0405259, U.S. Department of Energy DE-AC03-76SF00098, National Natural Science Foundation of China and Shanghai Science, and KICOS&MEST of Korea.

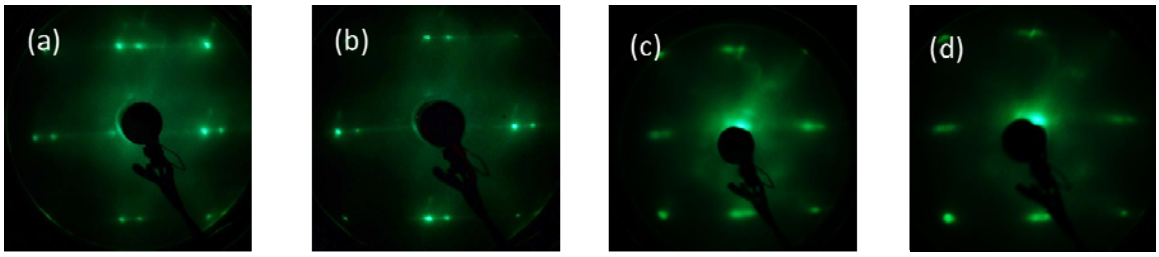

Fig. 1: (color online) LEED patterns taken at ~123 eV of at each stage of the FeMn(10ML)/Fe(2ML)/Co(20ML)/Cu(1,1,10) sample growth. (a) Cu(1,1,10) substrate, (b) after 20ML Co growth, (c) after 2ML Fe growth, and (d) after 10ML FeMn growth.

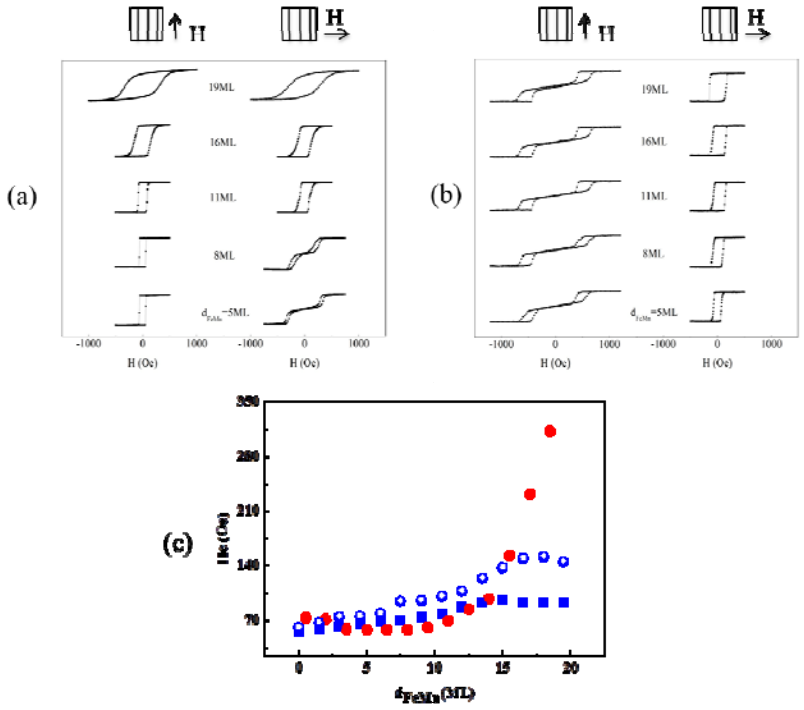

Fig. 2. (color online) (a) MOKE hysteresis loops of FeMn/Fe(2ML)/Co/Cu(1,1,10) at room temperature. (b) MOKE hysteresis loops of FeMn/Fe(8ML)/Co/Cu(1,1,10) at T=90K. (c) Coercivity of the easy axis loops for d_{Fe}=2ML sample at room temperature (red solid dots), d_{Fe}=8ML sample at room temperature (blue squares), and d_{Fe}=8ML sample at T=90K (blue open circles).

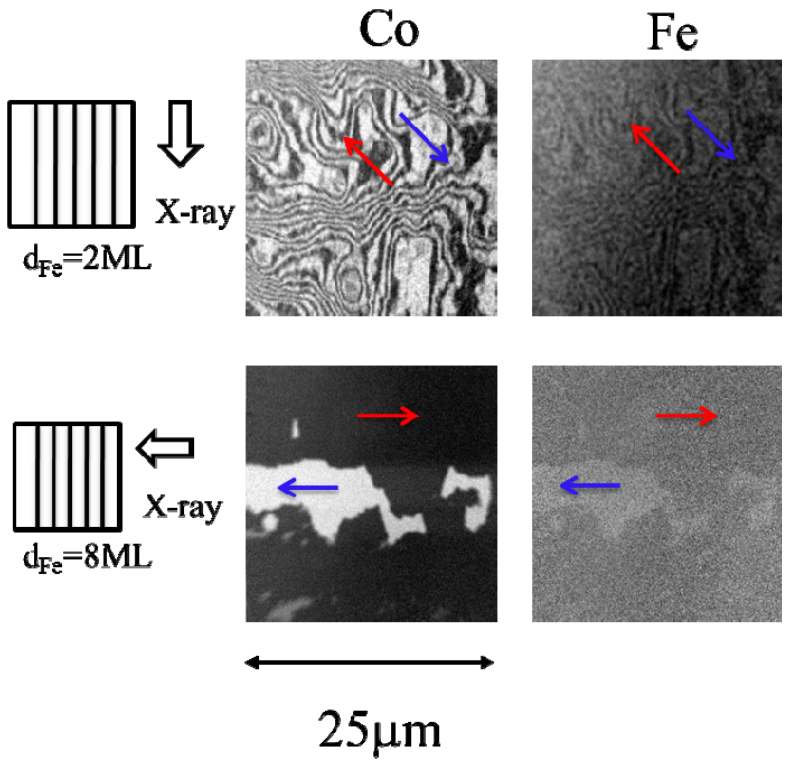

Fig. 3: XMCD-PEEM images (25µm×25µm) of FeMn/Fe/Co/Cu(1,1,10). The same domain pattern for Co and Fe shows that the FM fcc Fe at 2ML and the induced FM Fe in the AFM fcc Fe at 8ML are coupled ferromagnetically to the Co moment.

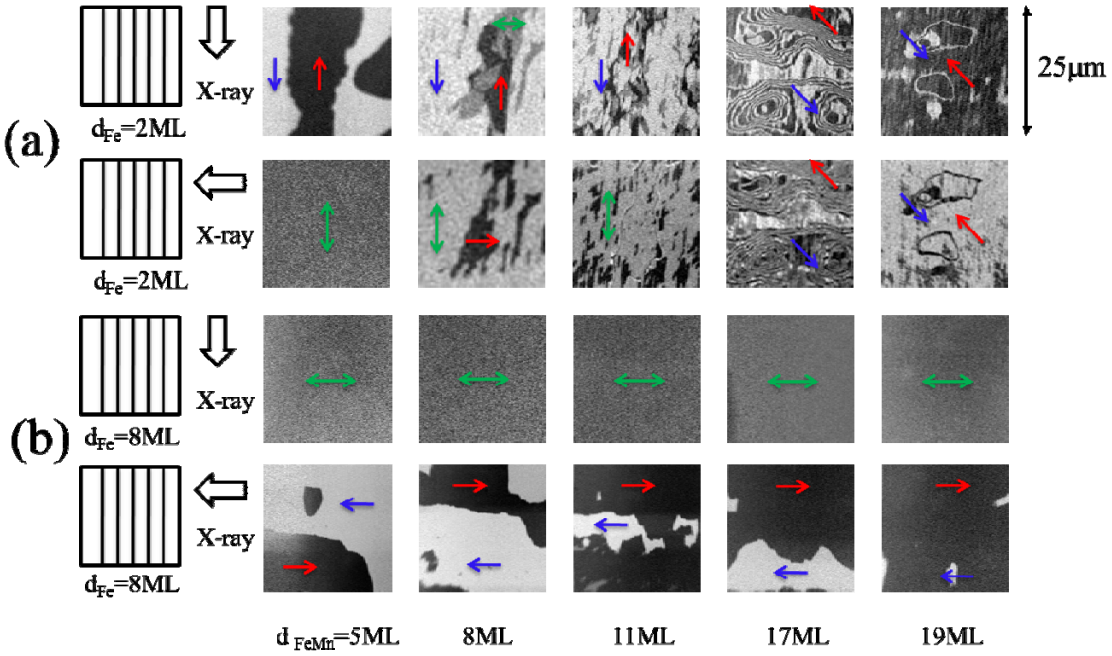

Fig. 4. XMCD-PEEM images (25μm×25μm) of FeMn/Fe/Co/Cu(1,1,10). The characteristic domain evolution in the FM phase fcc Fe (d_{Fe}=2ML) sample no longer exists in the AFM phase fcc Fe (d_{Fe}=8ML) sample. Each pairs of images are taken at the same positions of the sample.

References:

1. W.H. Meiklejohn and C. P. Bean, Phys. Rev. **102**, 1413 (1956).
2. B. Dieny, V. S. Speriosu, S. S. P. Parkin, B. A. Gurney, D. R. Wilhoit, and D. Mauri, Phys Rev. B **43**, 1297 (1991).
3. A. Berger and H. Hopster, Phys. Rev. Lett. **73**, 193 (1994).
4. N. C. Koon, Phys. Rev. Lett. **78**, 4865 (1997).
5. A. P. Malozemoff, Phys. Rev. B **35**, 3679 (1987).
6. V. I. Nikitenko, V. S. Gornakov, A. J. Shapiro, R. D. Shull, Kai Liu, S. M. Zhou, and C. L. Chien, Phys. Rev. Lett. **84**, 765 (2000).
7. V. S. Gornakov, Yu. P. Kabanov, O. A. Tikhomirov, V. I. Nikitenko, S. V. Urazhdin, F. Y. Yang, C. L. Chien, A. J. Shapiro, and R. D. Shull, Phys. Rev. B **73**, 184428 (2006).
8. T. Mewes, B. Hillebrands, and R. L. Stamps, Phys. Rev. B **68**, 184418 (2003).
9. Hyeok-Cheol Choi, Chun-Yeol You, Ki-Yeon Kim, Jeong-Soo Lee, Je-Ho Shim, and Dong-Hyun Kim, Phys. Rev. B **81**, 224410 (2010).
10. Yu. P. Kabanov, V. I. Nikitenko, O. A. Tikhomirov, W. F. Egelhoff, A. J. Shapiro, and R. D. Shull, Phys. Rev. B **79**, 144435 (2009).
11. F. Offi, W. Kuch, and J. Kirschner, Phys. Rev. B **66**, 064419 (2002).
12. D. Schmitz, E. Schierle, N. Darowski, H. Maletta, E. Weschke, and M. Gruyters, Phys. Rev. B **81**, 224422 (2010).
13. Wolfgang Kuch, Liviu I. Chelaru, Francesco Offi, Jing Wang, Masato Kotsugi, and. Jürgen Kirschner, Phys. Rev. Lett. **92**, 017201 (2004).
14. W. Kuch, F. Offi, L. I. Chelaru, M. Kotsugi, K. Fukumoto, and J. Kirschner, Phys. Rev. B **65**, 140408(R) (2002).
15. C. Won, Y. Z. Wu, H. W. Zhao, A. Scholl, A. Doran, W. Kim, T. L. Owens, X. F. Jin, and Z. Q. Qiu, Phys. Rev. B **71**, 024406 (2005).
16. J. Choi, J. Wu, Y. Z. Wu, C. Won, A. Scholl, A. Doran, T. Owens, and Z. Q. Qiu, Phys. Rev. B **76**, 054407 (2007).
17. J. W. Cai, W. Y. Lai, J. Teng, F. Shen, Z. Zhang, and L. M. Mei, Phys. Rev. B **70**, 214428 (2004).
18. W. Kuch, F. Offi, L. I. Chelaru, J. Wang, K. Fukumoto, M. Kotsugi, J. Kirschner, and J. Kuneš, Phys. Rev. B **75**, 224406 (2007).
19. Kohji Nakamura, Tomonori Ito, and A. J. Freeman, Phys. Rev. B **70**, 060404 (2004).

20. J. Wu, J. Choi, A. Scholl, A. Doran, E. Arenholz, Chanyong Hwang, and Z. Q. Qiu, Phys. Rev. B **79**, 212411 (2009).

21. R. K. Kawakami, M. O. Bowen, Hyuk J.Choi, Ernesto J. Escorcia-Aparicio, and Z. Q. Qiu, Phys. Rev. B **58**, 5924 (1998).

22. Dongqi Li, M. Freitag, J. Pearson, Z. Q. Qiu, and S. D. Bader, Phys. Rev. Lett. **72**, 3112 (1994).

23. Ernesto J. Escorcia-Aparicio, R. K. Kawakami, and Z. Q. Qiu, Phys. Rev. B **54**, 4155 (1996).

24. U. Bovensiepen, Hyuk J. Choi, and Z. Q. Qiu, Phys. Rev. B **61**, 3235 (2000).

25. G. Malcolm Stocks, W. A. Shelton, Thomas C. Schulthess, Balazs Ujfalussy, W. H. Butler, and A. Canning, J. Appl. Phys. **91**, 7355 (2002).

26. D. Qian, X. F. Jin, J. Barthel, M. Klaua, and J. Kirschner, Phys. Rev. Lett. **87**, 227204 (2001).

27. J. Wang, W. Kuch, L. I. Chelaru, F. Offi, M. Kotsugi, and J Kirschner, J. Phys.: Condens. Matter **16**, 9181 (2004).

28. Y. Z. Wu, C. Won, A. Scholl, A. Doran, F. Toyoma, X.F. Jin, N. V. Smith, and Z. Q. Qiu, Phys. Rev. B **65**, 214417 (2002).